지구물리 | Vol. 9, No. 3, Special Volume, pp. 273-286, 2006 | J Korean Geophysical Soc

Geoelectrical Structure of the Kyongsang Basin from Magnetotelluric Sounding

Choon-Ki Lee*, Heuisoon Lee, Byung-Doo Kwon*, In-Ky Cho***, Seokhoon Oh****, Yoonho Song***** and Tae-Jong Lee*******

**Seoul National University, Dept. Earth Science Education*
***Gyeongin National University of Education, Dept. Science Education*
****Kangwon National University, Dept. Geophysics*
*****Korea Institute of Water and Environment*
******Korea Institute of Geoscience and Mineral Resources*

ABSTRACT

The Kyongsang Basin is the most representative Cretaceous basin in the Korean Peninsula where extensive crustal deformation and non-marine sedimentation took place in the early Cretaceous period. The lithology of the basement of the basin and adjacent areas is comprised of mainly Precambrian gneiss complex and Mesozoic granite intrusions. We have carried out magnetotelluric (MT) surveys to investigate the deep geoelectric structure around the Kyongsang Basin. The MT data were collected in the frequency range from 0.00042 to 320 Hz at 24 sites along a profile across the northern part of Kyongsang Basin. The results of MT inversion show that the thickness of sediments is estimated about 3 km to 9 km and the depth to base of granite intrusion is about 20 km. A remarkable discovery in this study is the highly conductive layer beneath the basin, having the resistivity of 1 ohm-m to 30 ohm-m and the thickness of about 3 km to 4 km or more. Although we are not able to reveal the nature of this layer, the result of this study could provide some basic information with respect to the formation process and deposit environment of the proto-Kyongsang Basin.

Key words

Kyongsang Basin, magnetotllurics, geoelectrical structure, MT inversion

1. Introduction

The Kyongsang Basin is the largest Cretaceous basin in the southeastern part of the Korean peninsula. The stratigraphy and depositional environment of this basin have been investigated by many scientists (Chang, 1975; Chang, 1988; Choi, 1985). From their studies, it is commonly regarded that the basin was deposited under the fluvio-lacustrine condition throughout the basin history and the subsidence, sedimentation, block movement and igneous activity intimately related mutually. In addition, some information about the basin structure have been restrictively achieved by the gravity, magnetic and seismic studies (Kim *et al*, 2000; Kim *et al*, 2005). However, the resolution of geophysical surveys conducted for the basin is not enough to reveal the deep structure of basin clearly.

The prime goal of our research is to figure out the deep lithospheric structure of the Korean peninsula based on the geoelectrical properties investigated by using magnetotelluric (MT) methods. As a part of the regional research, we carried out the two-dimensional profile surveys across the Kyongsang Basin and established more reliable model of basin structure.

2. Geologic setting

The stratigraphic sequence of the Kyongsang Basin consists of three major lithostratigraphic groups: the lower Sindong Group confined in the western part of the basin, the middle Hayang Group characterized by the intercalation of basic and intermediate volcanic layers, and the upper volcanic Yuchon Group (Fig. 1). It is believed that the sedimentary layers were largely formed in fluvio-lacustrine environments on the Precambrian massif.

Petrological and sedimentological studies of the Kyongsang Basin suggest that the stratigraphic sequences

Corresponding Author : Choon-Ki Lee (cklee92@snu.ac.kr)
원고접수일 : 2006년 1월 16일 게재승인일 : 2006년 9월 26일

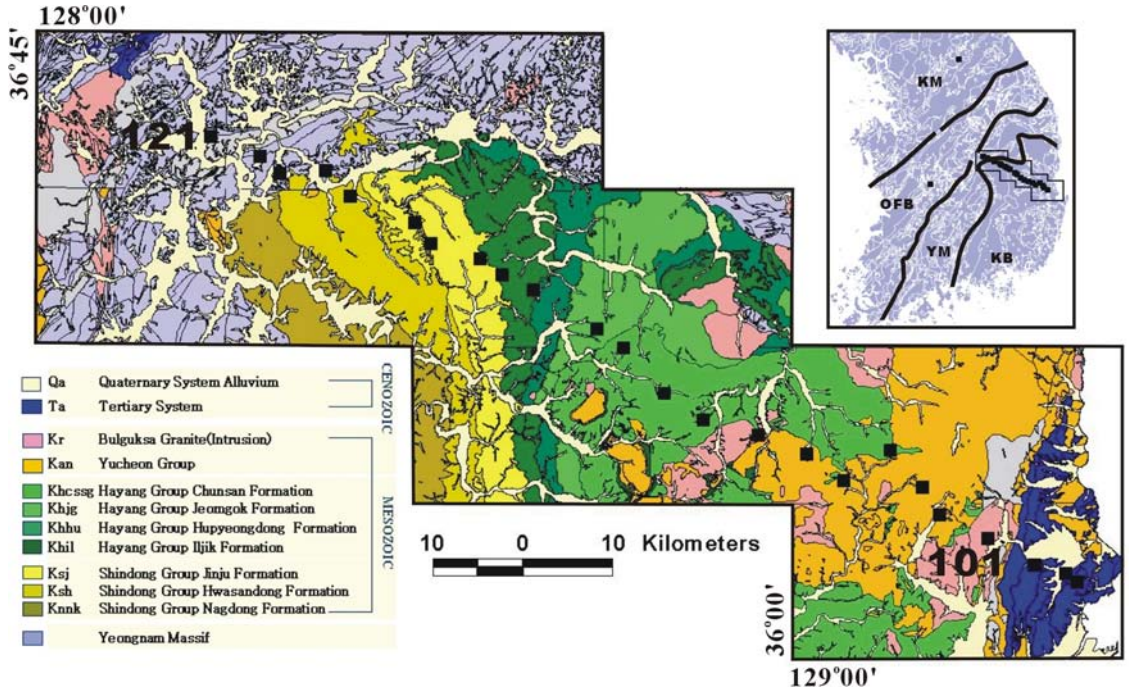

Fig. 1 Geologic map of the northern part of the Kyongsang Basin and location of the MT survey sites (filled square).

can be grouped into three facies associations: alluvial fan, flood plain, and lacustrine environments, including volcanic terranes and granite intrusive group (Chang, 1975; Choi, 1985). The occurrences of various fossils indicate that the basin was in saline lake under evaporative semiarid to arid conditions (Woo *et al*., 1991; Paik and chun, 1993). Deposition of the alluvial fan systems was strongly controlled by fault activity, while the distribution of the fluvial plain and lake systems was determined primarily by the change of precipitation and evaporation ratio (Choi, 1985).

During the Sindong period, extensional tectonism formed a north-northeastward plunging graben, which was bounded by the syndepositional Andong fault on the north margin. The alluvial fans were composed of numerous small fans which were formed at the terminals of small valleys developed in the upthrown lip areas (Fig. 2).

The Sindong group is composed of sandstone, shale, conglomerate and marl. The group is divided, primarily on the basis of variation in rock color, into the Nakdong (2,100-840 m thick), Hasandong (550-1,400 m thick) and Jinju (1,200-750 m thick) formation (Chang, 1988).

During the Hayang period, the basin expanded stepwise outside the proto-Kyongsang Basin by successive back

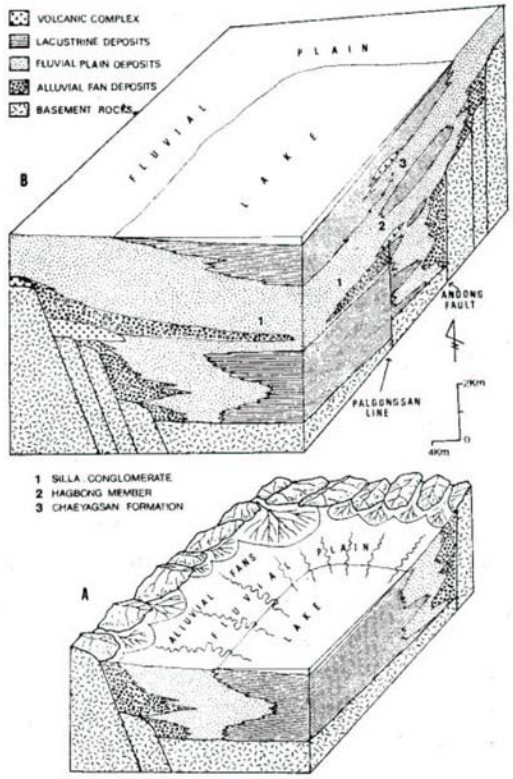

Fig. 2 Reconstruction of depositional framework. (A) at the end of the Sindong period. (B) at the end of the Hayang period (after Choi, 1985).

faulting, as supported by rapid basin subsidence, active volcanism, and lower maturity of the sediments as well as the wide distribution of the Hayang Group on the crystalline basement outside the basin. Accordingly, alluvial fan, fluvial plain, and lake systems were developed concentrically towards the basin center

The Hayang group is composed of shale, sandstone, and minor amount of marl and conglomerate derived from surrounding source areas with volcanic rocks extruded within the sedimentary area. The total thickness of Hayang group is 1,000 to 5,000 m.

The Yuchon volcanic group, 2,000 to 3,000 m thick, consists of abundant volcanic rocks and associated sedimentary rocks. It is in contrast to the underlying Hayang group that consists only a trivial amout of volcanic rocks. An erosional unconformity between the Hayang and the Yuchon Groups has been recently clarified in most places.

In the northwestern margin of Kyongsang Basin, the basin confronts Sobaeksan massif (a part of the Yongnam massif) comprised of Precambrian gneiss complex and Mesozoic granite intrusions. In the eastern part of the Kyoungsang Basin, the Tertiary Pohang Basin overlies Cretaceous sedimentary rocks. The Tertiary sediment formation is characterized by semi-consolidated mudstone.

3. Data aquisition and processing

The MT survey profile was aligned perpendicular to the strike of the principal geologic structure of the Korean peninsula (N30°E), so called 'China direction', although the boundary between the basin sediments and the gneiss complex has the direction of N85°E. Since the study area is close to the Okchon fold belt that is the representative tectonic structure of the peninsula, we presumed that the strike of deep structure is similar to the principal strike of the Korean Peninsula. The MT surveys with the spacings of 3-8 km were carried out at the 21 sites. In addition, Lee *et al*. (2004) densely acquired MT data in the Pohang Basin, eastern part of the profile, for the purpose of geothermal study. The data of only three sites in the Pohang Basin were used for the interpretation of 2-D structure of our study area. Therefore, the total length of the survey line is about 120 km (Fig. 1).

We used the MTU-5A system manufactured by Phoenix Geophysics Ltd. Two electric and three magnetic field components were measured using MTC-50 coil sensors and $Pb/PbCl_2$ electrodes. The measurement at each site was done for 15 hours during the nighttime from 08:00 (UT) to 23:00 (UT), showing relatively low cultural noises.

High noise levels result in the poorly determined and biased estimates of the MT impedance and tipper results. In order to minimize the bias due to the interference of noises, the additional EM fields were simultaneously acquired at the remote reference (RR) sites 70-170 km away from the local sites. Although the RR technique is applied, the impedances measured in the frequencies of 0.1-1 Hz band, so-called 'dead band', and the low frequency band are erroneous because the remote time series also contains some noises and the correlated noise signals are abundant. Therefore the bad data were removed before the procedure of inversion and interpretation as shown in the pseudosections of Fig. 3. The impedance selection (editing) relies on a thorough visual inspection of parameters such as apparent resistivity, phase, and tipper.

3.1 One-dimensional structure

On the MT profile, the width of basin is about 100 km and the maximum depth is expected about 9 km. Therefore, in some locations, the structure of the basin can be assumed as 1-D, which is composed of three layer, such as a shallow surface layer, a sedimentary layer, and the basement. Analysing the data collected from site 114 in the western part of the basin (Fig. 4a), it is apparent that the first layer is several hundred meters thick and has the resistivity of about 100 ohm-m. The second layer is a sedimentary layer about 4 km thick with the resistivity of several hundred ohm-m. The basement is highly conductive exhibiting resistivity of 3 ohm-m. In the eastern part of basin, the subsurface structure is very different from that in the western part. Although the data from the eastern part does not represent the responses of 1-D structure correctly, the 1-D inversion is valuable in assessing the range of the depth and resistivity scales. Interpreting the data of 106 sites as shown Fig. 4b, it is apparent that the resistivities of all layers in the eastern part are higher than those in the western part, and that the thickness of the second layer is about ten to twenty kilometers. Most sites are divided into the two groups represented by these two sites, and the MT

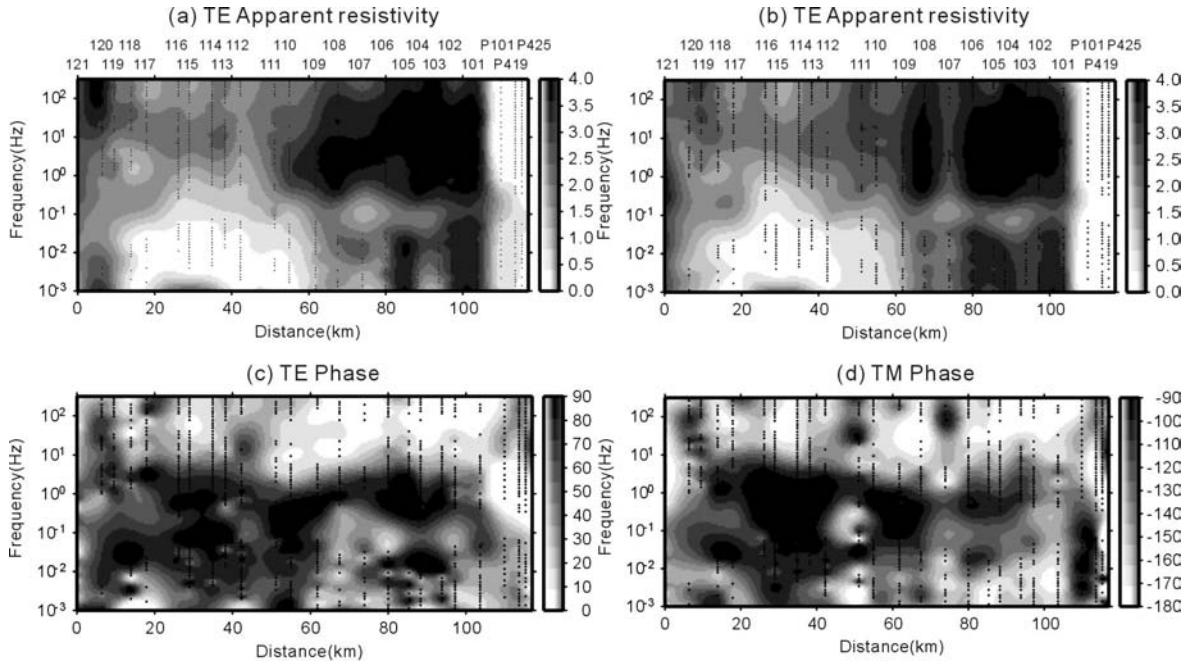

Fig. 3 The pseudo sections of apparent resistivity and phase after rotation, editing and static correction. The horizontal distance indicates the distance from site 121.

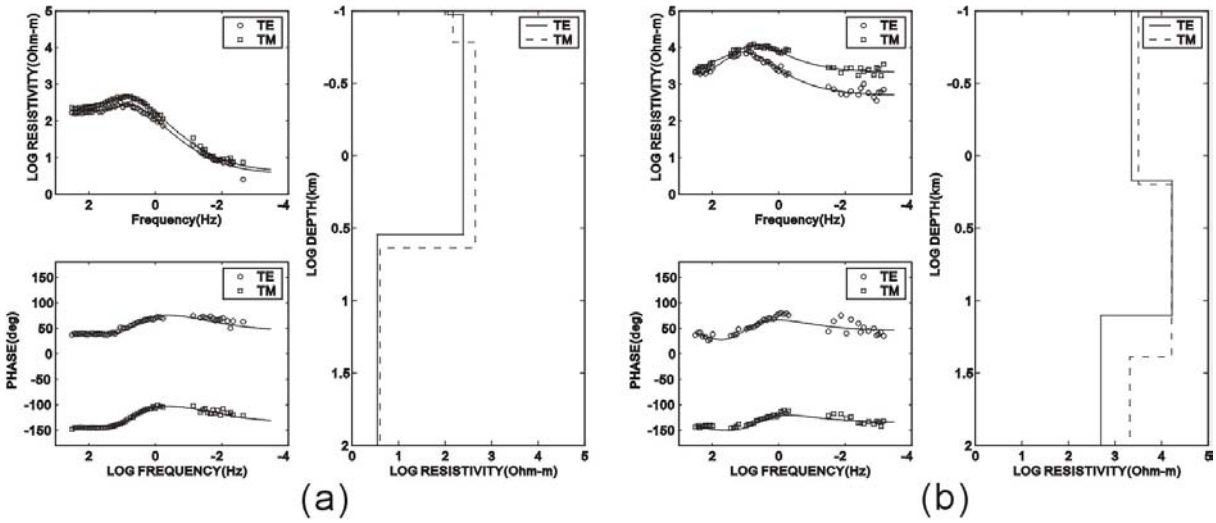

Fig. 4 MT data (left panels) and 1-D inversion result (right panel) from (a) the 114 site on the western part of basin and (b) the 106 site on the eastern part of basin. The two solid lines on the left panels are the theoretical responses to the 1-D layered models illustrated on the right panel.

responses slowly change in the zone including sites 108 to 110.

3.2 Dimensionality and directionality

The skew of the impedance tensor is generally used as an indicator of the dimensionality of geological structure. This is a measure of the ratio of its diagonal to off-diagonal elements. Normal skew is based on the magnitude of impedance tensor elements while phase sensitive skew relies on their phase information (Swift, 1967; Bahr, 1988). According to Bahr (1991), if the value of phase sensitive

skew is greater than 0.3, the data should be considered as the responses of 3-D structure. In the case of normal skew, the corresponding threshold is empirically 0.2. Fig. 5 shows the Swift and Bahr skew values for all sites. Very large skew values before impedance editing in the whole frequency band, especially between 1 Hz and 0.1 Hz, would be caused by the man-made electromagnetic noises. After editing, the skew values are below 0.2 (Swift) and 0.3 (Bahr) for $f > 1\ Hz$ at most sites while the values larger than 0.2 or 0.3 still remain for $f < 1\ Hz$.

Swift's method (1967) to determine the strike of a 2-D structure gives the analytical solution which depends on the magnitude of the impedances. Swift strike angles for all sites are plotted using rose diagrams for three different period ranges (Fig. 6). The strike angles are concentrated in the range of N0°-20°E and N80°-90°E in the low fre-

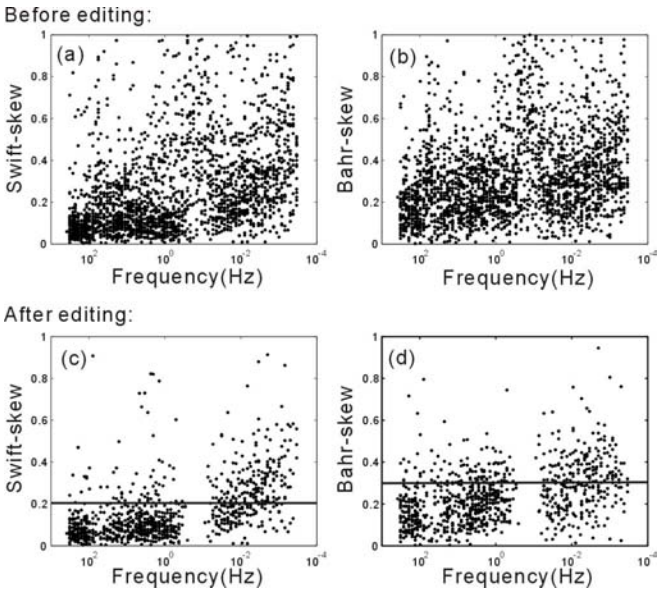

Fig. 5 Swift skew, (a) and (c), and Bahr skew, (b) and (d), for all sites before and after the impedance editing. The skew values are below 0.2 (Swift) and 0.3 (Bahr) for $f > 1\ Hz$ at most sites.

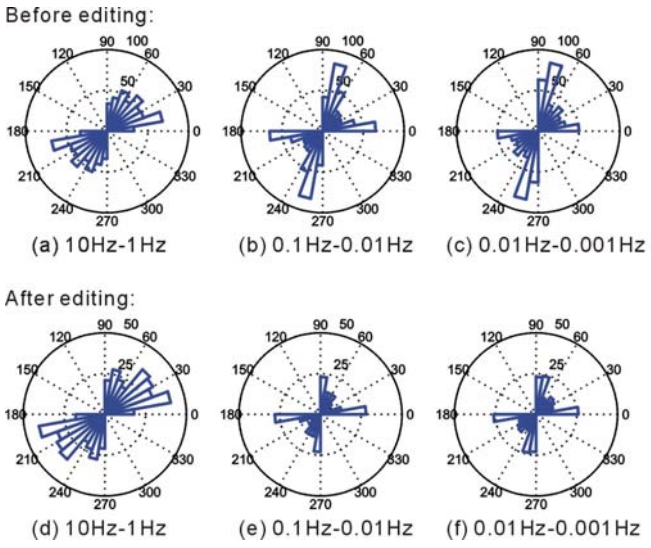

Fig. 6 Rose diagrams of Swift strike before editing (a-c) and after editing (d-f) at different frequency ranges. The strike angles are concentrated at approximately N0-20°E and N80°-90°E in the low frequency bands.

quency bands, but mostly undetermined in consideration of the ambiguity of 90° in the high frequency band.

On the other hand, magnetic field component is less sensitive to the shallow conductivity inhomogeneity than electric field component in the low frequency band. Accordingly, the geomagnetic transfer function is useful to assess the complexity of regional structure. The transfer function between the vertical and the horizontal magnetic field components can be expressed as real and imaginary induction vectors. The real vector, named as Pakinson induction arrow when reversed, usually points towards the region with higher conductivity (Parkinson, 1962). This vector implies that there must be lateral variations in electrical conductivity and the direction of vector is perpendicular to the strike of a 2-D structure. The induction arrows are shown in Fig. 7 along the MT profile. The strong induction arrows of eastern part mostly point the direction S60°E to S70E° due to the sea effect. These directions nearly coincide with the numerical modeling result of the sea effect due to East Sea (Yang, *et al*., 2003).

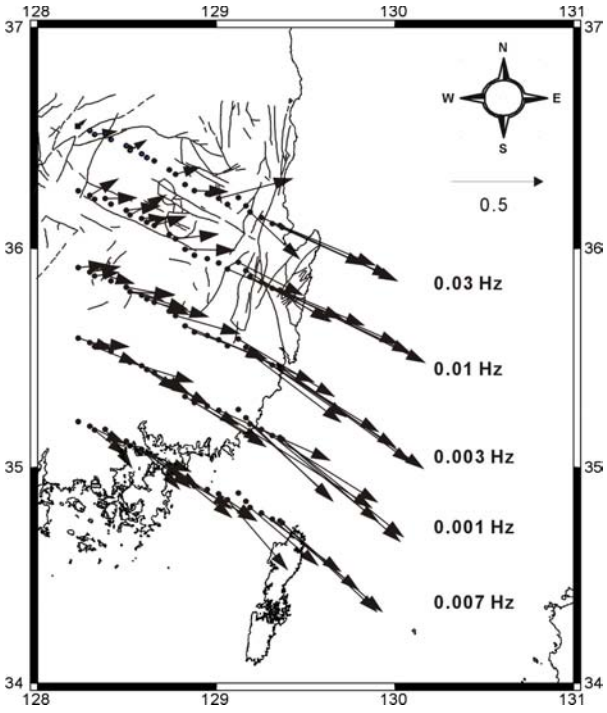

Fig. 7 Real induction arrows along MT profile for the five frequencies. All profiles except for the profile of 0.03Hz were shifted downward. The strong induction arrows mostly points toward the coastal line, under the influence of sea effect. Solid lines show the major fault in the study area.

Although the regional geological strike is NNE-SSW (China direction), there are two predominant lineament trends in Kyongsang Basin, N10°-30°E and N60°-80°W (Lee *et al*., 1984). Another locally prominent group of lineaments trend is N-N20°W. Lee *et al*.(1997) suggest that Kyongsang Basin is divided into five domains and sub-domains based on the most predominant direction of lineaments analyzed from satellite images. The western part of our MT profile is laid on a domain with predominant lineament strikes N50°-65°E and the eastern part belongs to a domain with strikes N20°-35°E (Fig. 7). However, the predominant strikes inferred from the impedance tensor are approximately N0°-20°E and N80°-90°E in the low frequency band. This strike trend is slightly different from the predominant lineament trends. This difference may be caused by the influence of the sea effect due to the N-S trending sea shore of East Sea because the MT data in the low frequency band contains the information about the more regional conductivity structure. When a current crosses a lateral resistivity boundary, it sets up and maintains a charge distribution on the resistivity boundary. These charges reduce the current density on the conductive side and increase the density on the resistive side. The changes of current density ultimately result in the changes of electric field and impedance. Accordingly, the charges accumulated along the N-S trending seashore can distort the strikes derived from the impedance tensor toward the direction of N-S. The magnetic field, however, is irrelevant to the charge accumulated on the boundary but more sensitive to the volumetric distribution of seawater. Therefore the directions of induction arrows do not exactly coincide with the direction perpendicular to the N-S trending land-sea boundary but rather point toward the southeast.

3.3 Static shift effect from near-surface heterogeneity

It is well known that the static shift effects cause serious difficulties in interpreting MT sounding curves (Kurtz *et al*., 1986; Jones, 1988). Static shift of an apparent resistivity curve is caused by an erroneous measurement of electric field due to the potential difference between the electrode pair not truly representing the horizontal electric field component because of the charges on the near-surface lateral boundaries.

Static correction techniques have been developed in two different approaches; the distortion-correction method and the hybrid method of MT and independent inductive geophysical measurement. Jiracek (1990) summarized the distortion-correction techniques: curve shifting (Park, 1985; Berdichevsky *et al.*, 1989), statistical or spatial averaging (Bostick, 1986; Beamish, 1990), and parameter constraints (Jones, 1988). Although, curve shifting and spatial averaging are relatively simple and rapid, these methods could obviously lead to erroneous results if the layer thicknesses change radically or the resistivity of the surface layer changes along the profile. In case there exist a layer within the sedimentary or other layered sequence whose electrical resistivity varies laterally in a fashion that can be described adequately by a simple parametric model, the parametric method proposed by Jones (1988) is less restrictive than any of those given above. In this paper, we adopted the latter method because the thickness of sedimentary layer varies from 3 km to 9 km and the granite intrusion makes not only the variation in layer thickness but also the lateral resistivity change in the layer in the study area.

From the field observations on the profile, we can derive a best-fitting 1-D model for each site and for both polarizations, i.e., both TE and TM mode. For the TE mode data, the model estimates of *i*th layer are

$$\rho_{TE,i}(x) = \rho_i(x) D_{TE}^{-2}(x) \quad (1)$$

$$d_{TE,i}(x) = d_i(x) D_{TE}^{-1}(x) \quad (2)$$

where $\rho_i(x)$ and $d_i(x)$ are the true resistivity and the true depth to base of *i*th layer, and $D_{TE}(x)$ is the real static-shift factor for the TE electric field at the location x.

In the correction procedure, There are two prior assumptions. One is that one of the layers in the sequence, the *i*th layer, can be represented in a parametric manner, and another is that the estimates of $\rho_i(x)$ vary in some statistical manner around the true value. The layer to be parameterized for correction procedure can be selected on the basis of statistical aspect of data or structural information of target area. In the selected *i*th layer, various parametric descriptions of their behavior with lateral distance are defined and then the static-shift factor, a constant offset, is derived from eq. (1) and (2). These factors are then employed to correct the depth of *i*th layer using

$$d^c_{TE,i}(x) = D_{TE}(x) d_{TE,i}(x) \quad (3)$$

Similar relationships of the TM mode data provide $D_{TM}(x)$ which is the static factor operating on the TM electric field.

After correcting the observed apparent resistivities using the derived static-shift factors, we can obtain the static-corrected apparent resistivities

$$\rho^c_{a,TE}(x,f) = D_{TE}(x)^2 \rho_{a,TE}(x,f) \quad (4)$$

and

$$\rho^c_{a,TM}(x,f) = D_{TM}(x)^2 \rho_{a,TM}(x,f) \quad (5)$$

at each frequency f.

The responses from all sites except for the three sites on the Pohang basin are shown in Fig. 8 where (a) is the E-polarization (TE) mode and (b) is the B-polarization (TM) mode data. Since there is a sharp contrast of resistivity between the Tertiary sediment of the Pohang basin and the neighboring Yuchon group, the assumption of gradual variation of horizontal layer, which is necessary for this static correction scheme, is not satisfied. Moreover, since the static shift is rarely observed at the sites on the Pohang basin, these sites are excluded in the correction procedure.

The apparent resistivity curves except for the sites on the Pohang basin are divided into two groups as mentioned previously. From not only the apparent curves but also the 1-D earth models, severe static-shift effects of up to one decade are obvious in each group. The 1-D earth models are inverted using the Marqurt-Levenberg minimization method with the three layer initial model, that is composed of the first layer with the thickness of 1km and the resistivity of 500 ohm-m, the second layer with 4 km and 1000 ohm-m, and the basement layer of 10 ohm-m. As a result, the first layer cannot be parameterized by any simple functions with the lateral distance because the resistivity and depth to the base of the first layer has nearly random variation. However, the resistivity and depth to base of second layer vary gradually and it seems to be able

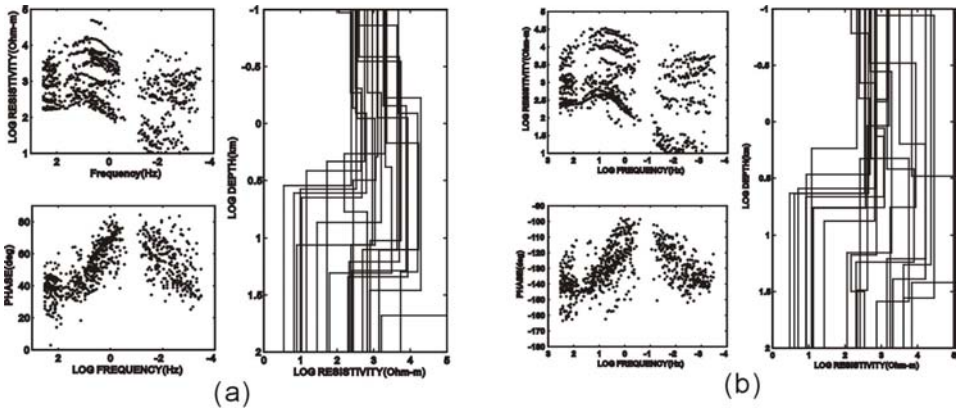

Fig. 8 MT data and 1-D models from all 21 locations along the profile: (a) the E-polarization data, and (b) the B-polarization data. The best fitting 1-D models from the apparent resistivity curves (upper-left panel) and the phase curves (lower-left panel) are shown in the right panel.

to fit the resistivity of second layer with a simple function. Fig. 9 shows the estimated $d_{TE,2}(x)$, $d_{TM,2}(x)$, $\rho_{TE,2}(x)$, and $\rho_{TM,2}(x)$ of second layer from 1-D inversion result.

For the parameterization of resistivity, the whole profile is zoned into three regions on the basis of the depths to the base of the second layer. The first region is the area containing 101 to 109 sites, which have large variations in depth and the shape of a bowl. In the second region containing 110 to 119 sites, an inclined layer obviously exists at the depth from 3 km to approximately 10 km. The layer in the third region westward from 119 site radically becomes deeper than that in the second region. This radical change indicates the boundary between the Kyongsang Basin and the Yongnam massif that is the basement of the basin.

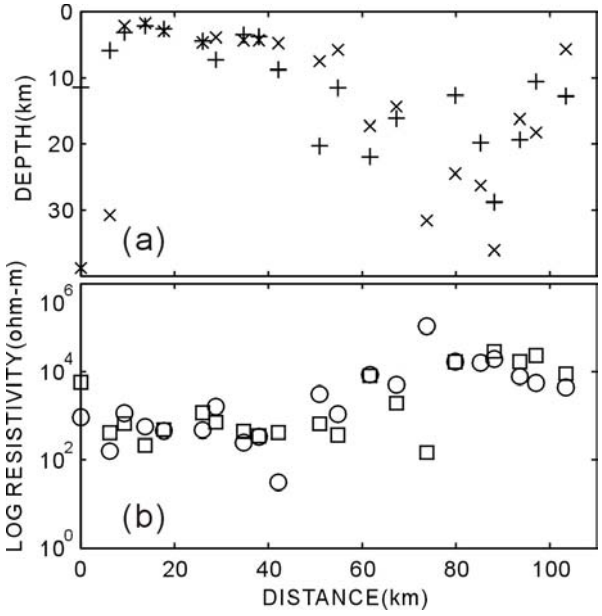

Fig. 9 Estimated $d_{TE,2}$ (+), $d_{TM,2}$ (×), $\rho_{TE,2}$ (○) and $\rho_{TM,2}$ (□) of the second layer using 1-D inversion result. The horizontal distance indicates the distance from site 121.

The parameter $\rho_{TE,2}(x)$ and $\rho_{TM,2}(x)$ are used for deriving the static shift factor using various parametric descriptions defined as third-order polynomial fitting, zonal mean, zonal first-order polynomial fitting and zonal second-order polynomial fitting. Fig. 10 shows the static corrected depths to the base of the second layer using the static shift factor calculated by eq. (1) and parametric functions as mentioned. The depths of basement layer in the second region are more linear in case of using zonal parametric functions than using the polynomial function defined in the whole profile. In addition to the linearity of layer, the range of the depth to the basement can more clearly describe, as suggested by geologists (Chang, 1988), that the maximum depth of the basin is about 9 km.

All zonal parametric function display similar results in the second region but, in the first zone, the distributions of the depths to basement are slightly different with respect to the parametric methods. In the case of zonal second-order polynomial fitting, the static correction makes a more smooth shape of basement because the resistivity of layer gradually changes in the form of a curve like a second-order polynomial. Finally, the apparent resistivity curves were shifted using the static shift factor derived from zonal second-order fitting and plotted in the pseudo-sections as shown in Fig. 3.

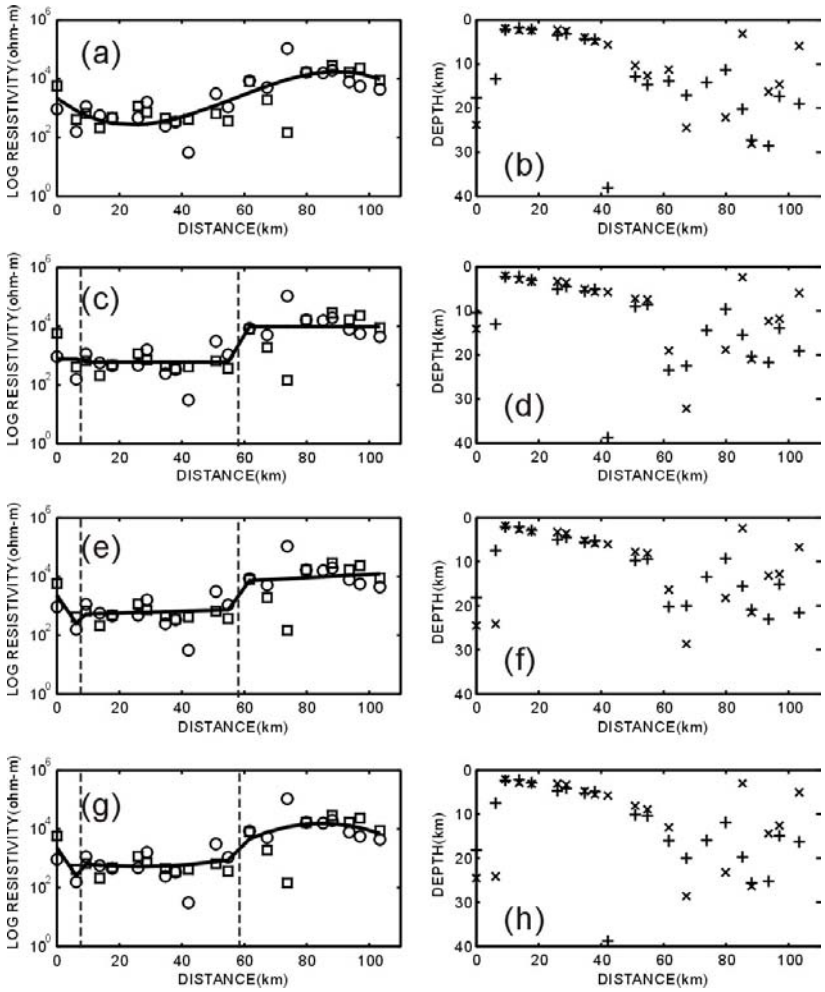

Fig. 10 Parametric functions of the apparent resistivity of the second layer (left) and the static corrected depths to the base of the second layer (right). Parametric descriptions of (a) third-order polynomial fitting, (c) zonal mean, (e) zonal first-order polynomial fitting and (g) zonal second-order polynomial fitting are applied.

4. Geoelectrical structure of the Kyongsang Basin

4.1 Two dimensional structure

As noted previously, the skew and strike data show that the electromagnetic fields at sites along a profile are influence by 3-D geologic structure and sea effect. Ultimately, it will be necessary to assess the influence of 3-D effect on the profile data by full 3-D modeling. The 2-D inversion of the profile is, however more easy and essential step to understand the subsurface structure and to construct a model of the geologic structure.

All apparent resistivity and phase data on the profile except for the 107 sites impacted by the local 3-D effect were inverted using the 2-D code of Rodi and Mackie (2001). The algorithm employs a nonlinear conjugate gradients (NLCG) method to search the minimum of an objective function that penalizes data residuals and second spatial derivatives of resistivity. The author's numerical experiments show that the algoritms based on conjugate gradients are more efficient than the Gauss-Newton algorithm in the aspect of both computer memory requirements and CPU time needed to find accurate solutions to the problems of realistic size. We compared the performances of the Occam (deGroot-Hedlin and Constable, 1990) and the REBOCC (Siripuvaraporn, 2000) inversion technique, that are well known algorithms of worldwide fame, to that of the NLCG. As a result, the NLCG method is tens times

faster than the Occam method but slightly slower than the REBOCC method. However, the resolution of the NLCG is higher than that of the REBOCC since it only uses an incomplete data set to increase the speed of processing.

The aim of the inversion is to find a reliable model, that minimizes a penalty function made up from a combination of misfit to the observations and the model roughness, in proportions determined by a parameter τ, starting from the initial model. Using the NLCG algorithm, considerable efforts should be made to explore a wide range of the parameters and the options which might influence the inversion (Tauber *et al*, 2003). Their effects were tested by examining the RMS misfits with respect to the initial background resistivities and the roughness parameters (Fig. 11). As a result, the inversion using the initial model with the background resistivity of 1000 ohm-m and the roughness parameter $\tau = 5$ results in the best result in the view of RMS error. In addition, to test the inversion characteristics of the subset of data, the inversions using TE, TM, and both mode data were calculated. Since the TM mode data have the best qualities with smaller error bars and biases, the RMS error of the case using this mode alone is lower than those of other two cases.

It is however difficult to say that the model with the lowest RMS error is the best reliable model because of the non-uniqueness of inversion. For more reliable models, we compared the results of the inversions using various parameters in Fig. 12, Fig. 13 and Fig. 14. Firstly, Fig. 12 shows the TM mode inversion result with the initial background resistivity of 10, 100, 1000, and 10000 ohm-m respectively. Although the RMS misfits are similar, the results with the initial background resistivity of 100 and 1000 ohm-m are a little bit different from the others. In the case of 100 ohm-m, the lower zone of highly conductive layer beneath 111 to 119 site seems to be emphasized relatively. In practically, the deep part under the conductive layer is not able to be resolved because the frequency range is not sufficient to confine the resistivity beneath the highly conductive layer. Secondly, TM mode inversions with the roughness parameter τ of 1, 5, 10 and 30 were tested (Fig. 13). The initial background resistivity is 1000 ohm-m. When τ is small, the emphasis is on achieving a good fit, which requires a rough structure. When τ is large, the emphasis is on finding a smooth model, which

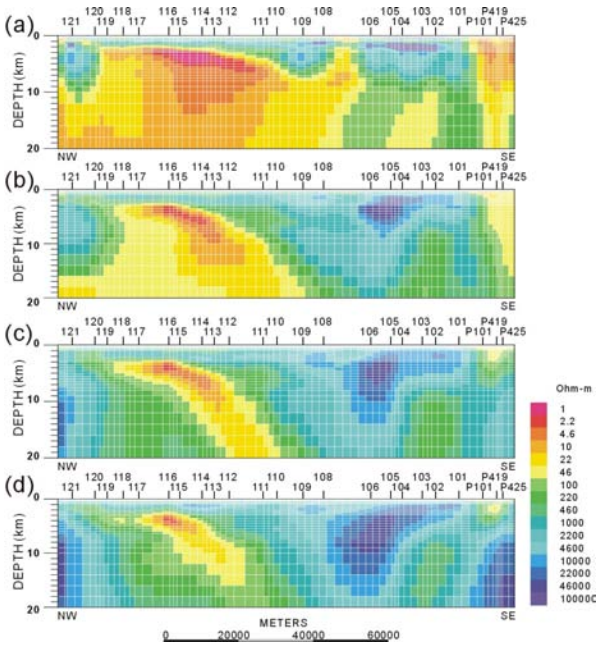

Fig. 12 TM mode inversion results with the initial background resistivities of (a) 10, (b) 100, (c) 1,000, (d) 10,000 ohm-m. The roughness parameter τ is 5.

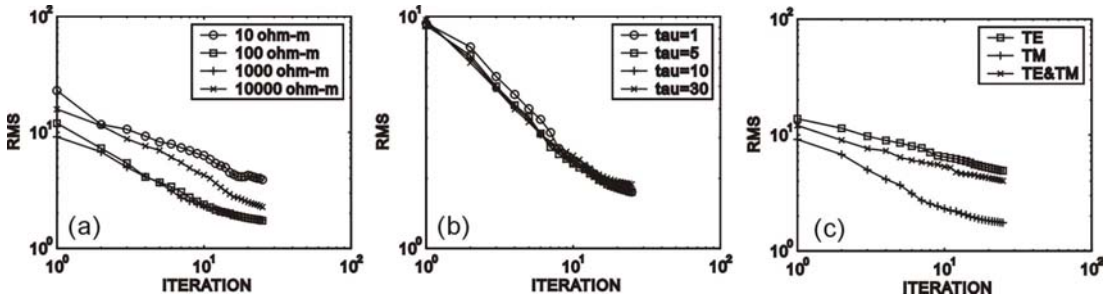

Fig. 11 RMS errors during the inversion process (a) with various initial background resistivities and (b) with various roughness parameters and with (c) the subset of the data.

may yield a rougher fit. Except for the case of $\tau = 1$, the results are acceptable because the top of highly conductive layer has the shape of a horizontal layer with a slope as the result of 1-D inversion. Finally, Fig. 14 shows the resistivity models fitting the TE mode, TM mode, and both modes together. The result from TE mode alone more accurately describes the linear shape of the top margin of highly conductive layer than that from TM mode alone. In contrast, the thickness of highly conductive layer seems to be more emphasized than that in case of using TM mode data. From the test of various inversions, we concluded that the TM mode inversion with the initial background resistivity 1000 ohm-m and $\tau = 5$ is best to interpret the geologic structure of the basin since the TM mode inversion does not only show the best RMS errors but also better confines layered structure of the sedimentary basin.

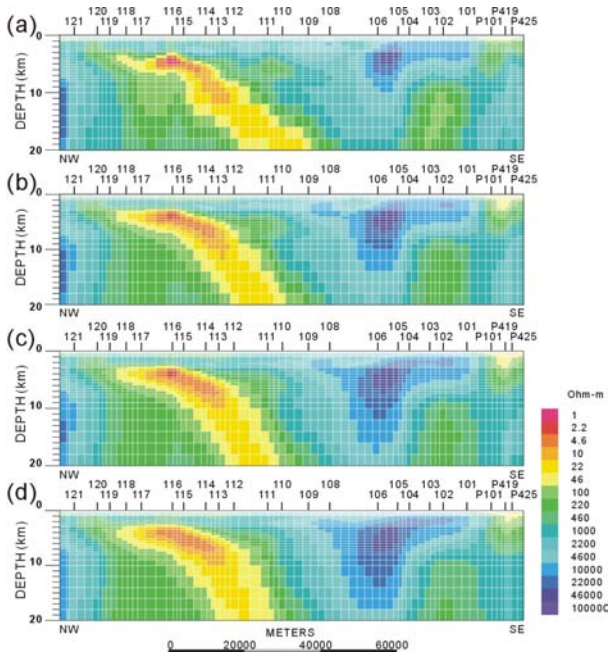

Fig. 13 TM mode inversion results with the roughness parameter of (a) 1, (b) 5, (c) 10 and (d) 30. The initial background resistivity is 1,000 ohm-m.

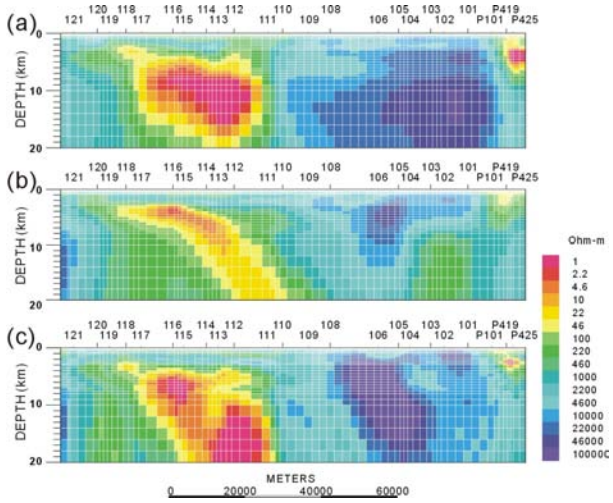

Fig. 14 Resistivity models fitting (a) TE mode data alone and (b) TM mode data alone, and (c) both mode data together.

4.2 Geophysical and geological interpretation

The geoelectric structure of the Kyongsang Basin result from the MT data shows three lateral contrasts of resistivity. First, the contrast between 118 site and 120 site indicates the front of the sedimentary basin toward the massif. In this region, the E-W trending Andong fault system separates the Kyongsang Basin from the Yongnam massif. The Andong fault had a largely reverse motion in which the hanging wall mainly moved toward the southeast and partly toward the south. The ages of pre- and post-reverse faulting plutons indicate that the reverse movement of the Andong fault system occurred between the Cretaceous and the early Tertiary times (Choi *et al*, 2002). Second, the variation between 108 site and 110 site is consistent with the lateral change of the lithostratigraphic unit of Kyongsang Basin. In this region, the facies change from the fluvio-lacustrine sedimentary layer of the Sindong group or partly of Hayang group to the volcanic dominant layer of Yucheon group is distinct. The lateral resistivity change due to the facies transition is enlarged by the resistive granite intrusions named as 'Bulgugsa' granite. The thickness of the sedimentary layer is estimated about 3 km to 9 km and the depth to the base of the granite intrusion is about 20 km. The last lateral contrast between 101 site and P101 site implies the sharp boundary between the Cretaceous and the Tertiary sediments and the extent of the Yangsan fault that is the biggest fault in the southeastern part of the Korean peninsula. Fig. 15 shows the geological model of the Kyongsang Basin based on the 2-D resistivity model derived from the inversion of the TM mode data alone.

Another remarkable feature of the MT response is the highly conductive zone at the frequencies less than 1 Hz.

The apparent resistivity at those frequencies reaches to about 1 ohm-m in the east part of the survey line between 111 and 119 site. The result of 1-D inversion reveals that the highly conductive zone from 3 km to 9 km depth is the horizontal basement overlayed by more resistive sedimentary layer with a slope of about 1/10. From the 2-D inversion profile, we are also able to find the highly conductive zone of 1 ohm-m to 30 ohm-m beneath more resistive layer with the thickness of 3 km to 9 km. Since the margin of the anomalous zone corresponds to the boundary between the Yongnam massif and the Sindong group of the Kyongsang Basin, it is thought that the conductive zone is correlated with the structure of lower part of the basin. The thickness of anomalous zone is estimated to be about 3 km to 4 km. We cannot however clearly define the lower bound of the zone because the frequency range is not sufficient to confine the resistivity beneath the highly conductive layer.

In the early Cretaceous, the northward subduction of the Izanagi Plate caused sinistral, brittle shearing in a retroarc setting accompanied by a number of pull-apart basins (Chun and Chough, 1992). The Kyongsang Basin was also a continental graben which was confined to so called proto-Kyongsang Basin during the Sindong period and expanded by successive back faulting during the Hayang period (Choi, 1986). In the view of stratigraphy, it is commonly regarded as that the basin is bounded below by the unconformity that represents the late Jurassic Daebo orogeny, the severest orogeny in Korea since the late Precambrian time. The pre-Cretaceous strata were intensely folded by the Daebo movement but the Cretaceous and Tertiary strata are only loosely folded and block-faulted.

The highly conductive zone may be formed after the Daebo orogeny since the anomalous zone appears not to be intensely folded in consideration of the layered shape and the low dip angle. Moreover, since its margin to the north coincides with the Andong fault, the formation of anomalous zone must be related with the development of the Kyongsang Basin.

On the other hand, let us consider the possibility that the lower formation of the Sindong group, named Nagdong formation, has extremely low resistivity. The formations in the Sindong group are divided into the sedimentary environments evolving from the alluvial fan (Nagdong formation) through floodplain (Hasandong formation) to lacustrine (Jinju formation). The Nagdong and the Hasandong formation have similar compositions, of conglomerate,

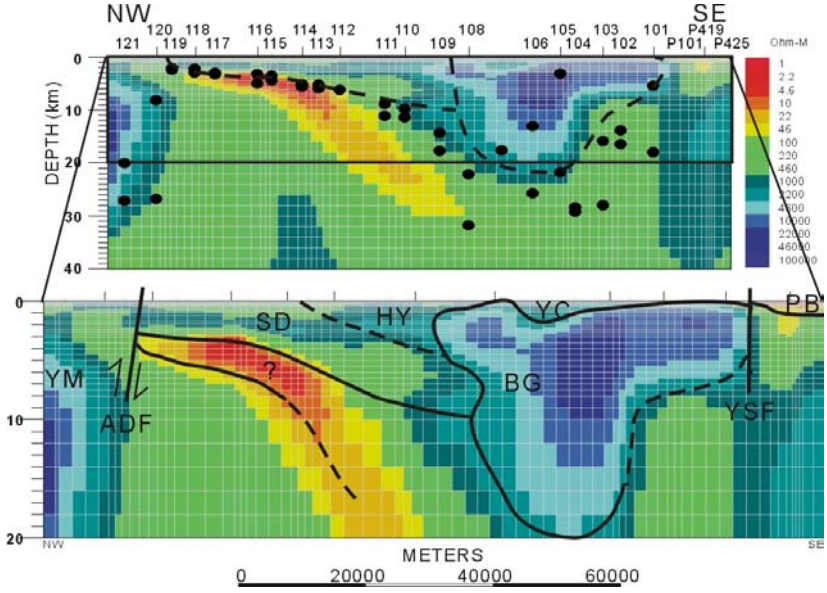

Fig. 15 Geological model of Kyongsang Basin based on the 2-D resistivity model derived by inverting the TM mode data alone. Solid circles shows the depths to base of second layer of the 1-D inversion result shown in Fig. 10h. YM, Yongnam massif; SD, Sindong group; HY, Hayang group; YC, Yuchon group; BG, Bulgugsa granite intrusion; PB, Pohang basin; ADF, Andong fault; YSF, Yangsan fault.

sandstone, siltstone and shale, except that the latter is a red-banded formation and the former is non-red strata. Therefore, we can expect that the resistivities of two formations are not severely different.

From the above discussion, the anomalous zone seems to be formed in the period between the Daebo orogeny and the deposition of Nagdong formation. In conclusion, we suggests a possibility that the highly conductive zone is caused by the structural deformation, making many faults and fractures, due to brittle shearing and the earliest deposition prior to Nagdong formation under the saline lake environment.

5. Conclusions

The basin structure result from the MT data is characterized by the lateral contrasts of resistivity to the marginal fault between the sedimentary basin and the Yongnam massif, the lateral change of the lithostratigraphic unit including the granite intrusion, and the sharp boundary between the Cretaceous and the Tertiary sediments. From the 1-D and 2-D inversions, the thickness of the sedimentary layer is estimated about 3 km to 9 km and the depth to the base of the granite intrusion is about 20 km. Another remarkable feature of basin structure is the highly conductive layer having the resistivity of 1 ohm-m to 30 ohm-m beneath the more resistive sedimentary layers with 3 km to 9 km thickness. In consideration of the geological environment, the anomalous layer seems to be formed in the period between the Daebo orogeny and the deposition of Nagdong formation, that is the lowest strata of the basin.

Based on this result, further geophysical and geological researches could provide some more interesting information with respect to the formation process and the deposit environment of the proto-Kyongsang Basin. First of all, it may be necessary to assess the influence of 3-D effect using full 3-D survey and modeling since the skew and induction arrow show the influence of 3-D induction due to the geological structure and sea effect.

Ackknowledgements

This work was supported by General Research Grants of Korea Science and Engineering Foundation (R01-2003-000-10340-0).

References

Bahr, K., 1988, Interpretation of the magnetotelluric impedance tensor: regional induction and local telluric distortion, J. Geophys., 62, 119-127.

Bahr, K., 1991, Geological noise in magnetotelluric data: a classification of distortion types, Phys. of Earth Planet. Int., 66, 24-38.

Beamish, D., 1990 A deep geoelectric survey of the Carnemenellis granite, Geophys. J. Int., 102, 679-693.

Berdichevsky, M. N., Vanyan, L. L., and Dmitriev, V. I., 1989, Methods in the U.S.S.R. to reduce near-surface inhomogeneity effects on deep magnetotelluric sounding, Phys. Earth Planet. Int., 53, 194-206.

Bostick, F. X., 1986, Electromagnetic array profiling, 56th Annu. Int. Mtg. Soc. Explor. Geophys., Exp. Abstr., 60-61.

Chang, K. H., 1975, Gretaceous stratigraphy of Southeast Korea, J. Geol. Soc. Korea, 11, 1-23.

Chang, K. H., 1988, Gretaceous stratigraphy and paleocurrent analysis of Kyongsang Basin, Korea, J. Geol. Soc. Korea, 24, 194-205.

Choi, H. I., 1985, Sedimentology and its implications for stratigraphic classifications of the Cretaceous Gyeongsang basin, J. Geol. Soc. Korea, 21, 26-37.

Choi, H. I., 1986, Sedimentation and evolution of the Cretaceous Gyeongsang Basin, southeastern Korea, J. Geol. Soc. London, 143, 29-40.

Choi, P. Y., Lee, S. R., Choi, H. I., Hwang, J. H., Kwon, S. K., Ko, I. S., An, G. O., 2002, Movement history of the Andong Fault System: Geometric and tectonic approaches, Geosciences Journal, 6, 91-102.

Chun, S. S. and Chough, S. K., 1992, Tectonic history of Gretaceous sedimentary basins in the southwestern Korean Peninsula and Yellow sea. In: Chough, S. K. (ed.) Sedimentary Basins in the Korean Peninsula and Adjacent Seas, Hanlimwon, Seoul, 104-128.

deGroot-Hedlin, C. and Constable, S., 1990, Occam's inversion to generate smooth, two-dimensional models from magnetotelluric data, Geophysics, 55, 1613-1624.

Jiracek, G. R., 1990, Near-surface and topographic distortions in electromagnetic induction, Surv. Geophys., 11, 163-203.

Jones, A. G., 1988, Static shift of magnetotelluric data and its removal in a sedimentary basin environment, Geophysics, 53, 967-978.

Kim, W. K., Min, K. D., Won, J. and Kim, J. W., 2000, Geologic structure of Euiseong sub-basin from spectrally correlated geopotential field anomalies, Econ. Environ. Geol., 33, p. 217-228

Kurtz, R. D., Ostrowski, J. A., and Niblett, E. R., 1986, A magnetotelluric survey over the East Bull Lake Gabbro-Anorthosite

complex, J. Geophys. Res., 91, 7403-7416.

Lee, B. J., Chwae, U. C. and Kang, P. C., 1997, Lineaments in the southeastern part of the Korean Peninsula, J. Geol. Soc. Korea, 33, 18-26.

Lee, K., Jeong, B., Kim, Y. and Yang, S. J., 1984, A geophysical study of the Yangsan fault area, J. Geol. Soc. Korea, 20, 222-240.

Lee, T. J., Song, Y., Uchida, T., Mitsuhata, Y., Oh, S. and Graham, G. B., 2004, Sea effect in three-dimensional magnetotelluric survey: An application to geothermal exploration in Pohang, Korea, Proceeding of the 7th SEGJ International Symposium, November 2004, Sendai, 279-282.

Paik, I. S. and Chun, J. H., 1993, Laminar calcretes, calcrete pisoids and ooids, and rhizoliths from the Kyeongsang Supergroup, Korea, J. Geol. Soc. Korea, 29, 108-117.

Park, S. K., 1985, Distortion of magnetotelluric sounding curves by three-dimensional structures, Geophysics, 50, 785-797.

Parkinson, W. D., 1962, The influence of continents and oceans on geomagnetic variations, Geophys. J. R. Astro. Soc., 6, 441-449.

Rodi, W., and Mackie, R. L., 2001, Non-linear conjugate gradients algorithm for 2-D magnetotelluric inversion, Geophysics, 66, 174-187.

Siripuvaraporn, G., 2000, An efficient data-subspace inversion method for 2-D magnetotelluric data, Geophysics, 65, 791-803.

Swift, C., 1967, A magnetotelluric investigation of an electrical conductivity anomaly in the southweatern United States, Ph.D. Thesis, MIT Press. Cambridge, MA.

Tauber, S., Banks, R., Ritter, O., and Weckmann, U., 2003, A high-resolution magnetotelluric survey of the Iapetus Suture Zone in southwest Scotland, Geophys. J. Int., 153, 548-568.

Woo, K. S., Lee, K. C., Paik, K. H., 1991, Gretaceous lacustrine radial ooids in the Kyongsang Basin, Korea: paleoclimatic implications, J. Geol. Soc. Korea, 27, 171-176.

Yang, J., Oh, S, Lee, D. K., Kwon, B. D. and Youn, Y. H., 2003, The 3-D geomagnetic induction modeling and the application of difference arrow considering with conductivity structures on the Korean Peninsula, Jour. Korean Earth Science Society, 24, 440-448.